Surface Review and Letters, Vol. 24, No. 7 (2017) 1750104 (13 pages)

DOI: 10.1142/S0218625X17501049

INFLUENCE OF ANNEALING TEMPERATURE ON THE CHARACTERISTICS OF NANOCRYSTALLINE SnO_2 THIN FILMS PRODUCED BY Sol–Gel AND CHEMICAL BATH DEPOSITION FOR GAS SENSOR APPLICATIONS

SELMA M. H. AL-JAWAD*,‡, ABDULHUSSAIN K. ELTTAYF† and AMEL S. SABER†

*School of Applied Sciences, University of Technology, Baghdad, Iraq

†Ministry of science and technology, Iraq

‡salma-aljawad@yahoo.com

Received 6 May 2016
Revised 8 January 2017
Accepted 7 February 2017
Published 9 March 2017

Pure nanocrystalline SnO_2 films were grown on a clean glass substrate by using sol–gel dip coating and chemical bath deposition (CBD) techniques for gas sensor applications. The films were annealed in air at 300°C, 400°C, and 500°C for 60 min. The deposited films with a thickness of approximately 300 ± 20 nm were analyzed through X-ray diffraction, scanning electron microscopy (SEM), atomic force microscopy (AFM), and optical absorption spectroscopy. Results revealed that the films produced by dip coating exhibited a tetragonal rutile structure and those produced by CBD showed a tetragonal rutile and orthorhombic structure. The crystalline sizes of the films produced by dip coating annealed at 300°C, 400°C, and 500°C were 8, 14, and 22.34 nm and those for CBD films at these temperatures were 10, 15, and 22 nm, respectively. AFM and SEM results indicated that the average grain size increased as annealing temperature increased. The transmittance and absorbance spectra were then recorded at wavelengths ranging from 300 nm to 1000 nm. The films produced by both the methods yielded high transmission at visible regions. The optical band gap energy of dip-coated films also increased as annealing temperature increased. In particular, their optical band gap energies were 3.5, 3.75, and 3.87 eV at 300°C, 400°C, and 500°C, respectively. By comparison, the energy band gap of CBD-prepared films decreased as annealing temperature increased, and their corresponding band gaps were 3.95, 3.85, and 3.8 eV at the specified annealing temperatures. The films were further investigated in terms of their sensing abilities for carbon monoxide (CO) gas at 50 ppm by measuring their sensitivity to this gas at different times and temperatures. Our results demonstrated that dip-coated and CBD-prepared films were highly sensitive to CO at 200°C and 250°C, respectively.

Keywords: SnO_2 thin films; sol–gel; chemical bath deposition; XRD; SEM; AFM; CO gas sensor.

1. Introduction

SnO_2 known by the systematic name tin (IV) oxide is an n-type semiconductor.[1] SnO_2 films are used as transparent conducting electrodes in many electro-optic applications, such as liquid crystal and optoelectronic devices.[2] Compared with other materials,

‡Corresponding author.

SnO_2 exhibits a large band gap of 3.6–4.0 eV[3–5] and provides remarkable advantages, such as low temperature increase and high chemical stability. SnO_2 is also used for different applications, including heat mirrors and solar energy conversion devices. Some examples of thin-film transparent oxide semiconductors include SnO_2, SnO_2:F, SnO_2:Sb, SnO_2:In, and $CdSnO_4$. SnO_2 thin films have been utilized as a window layer in solar cells and in other applications, including sensors for CO, H_2S, H_2, NO, and CH_4 gases.[2,3] SnO_2 films can be deposited through different methods, including DC magnetron sputtering,[4] ion beam sputtering deposition,[5] dip coating and spin coating sol–gel processes,[6–8] chemical vapor deposition,[9] pyrolysis deposition,[10] and chemical bath deposition (CBD).[11] In our study, sol–gel and CBD were selected to prepare nanocrystalline SnO_2 films because they are well-known low-temperature aqueous methods used to deposit large-area films of semiconductors directly. These methods also provide several advantages, such as potential use of high-purity starting materials. Additionally, they involve cost-effective and simple processes and do not require vacuum equipment.[12]

Exposure to high CO concentrations can cause death. Low CO concentrations are similarly harmful to individuals with heart disease; in some instances, 1600 ppm CO causes headache, tachycardia, dizziness, and nausea within 20 min and death within 30 min.[13] CO also contributes to the formation of ground-level ozone and smog. This phenomenon causes respiratory problems. As such, CO must be detected to monitor environmental conditions. Maosong *et al.*[14] focused on the CO sensing properties of SnO_2 thin films. Williams *et al.*[15] used SnO_2 thin film to sense CO from a car exhaust and found that the sensor efficiently operates at 125°C. Kumar *et al.*[16] prepared SnO_2 thin films on a clean glass substrate by using a sol–gel dip incrustation technique at an annealing temperature of 500°C and determined the CO sensing properties of these films at different heat ranges. They found that grain size plays a vital role in gas sensing and these films are highly sensitive to 50 ppm CO at 220°C. Vaezi and Zameni[17] prepared SnO_2 thin films on soda–lime glass substrates by using a dip coating sol–gel method. After exposing the gas to different ethanol concentrations, they observed that films with a thickness of approximately 299 nm elicit optimum sensing responses at 300°C, 27.7 ppm ethanol (C_2H_5OH), 70 s response time, and 88 s recovery time. Tripathy *et al.*[18] deposited SnO_2 thin films on a glass substrate through thermal evaporation and sol–gel techniques for gas sensing applications and examined the structural, microstructural, optical, and gas sensing properties of these films. They found that thermally evaporated and sol–gel-prepared films are highly sensitive at 220°C and 235°C at 50 ppm, respectively. In this study, SnO_2nanostructured films were deposited and characterized through sol–gel dip coating and CBD. The CO sensing properties of these films were also evaluated as a function of annealing temperature.

2. Experimental

2.1. *Preparation of solution and deposition of the films by using dip coating method*

SnO_2 films were prepared using the following procedure. Chloride dehydrate ($SnCl_2 \cdot 2H_2O$; 2 g) was dissolved in C_2H_5OH (15 mL). The solution was stirred by a magnetic stirring apparatus for 1 h at 75°C–80°C. Then, the sol was mixed with glycerin ($C_3H_8O_3$) as a dispersion stabilizer to obtain the sol–gel for dip coating. Actually, this method preferred to rely on using films from the solution (sol) to be applied in dip-coating technique. The substrate glass slides at a dimension of 26 mm × 76 mm × 1 mm are cleaned by immersing in ultrasonic bath for 5 min and finally rinsed by ethanol. Thus, all films are dipped into the sol then slowly withdrawn from the bath at a fixed speed equal to 80 mm/min. All the films were dried at low temperature reaching 100°C at 30 min. Then, they are subjected to heat treatment at 300°C, 400°C, and 500°C for 60 min.

2.2. *Preparation of solution and deposition of the films using chemical bath deposition method*

The chemical bath system was used to prepare tin oxide SnO_2 thin films when they were dissolved separately. Up to 5.64 g of $SnCl_2 \cdot 2H_2O$ in 25 mL of distilled water and 1 g of sodium hydroxide in 25 mL of distilled water were then added. The molar concentrations of these compounds are 1 and 1 M, respectively. Subsequently, 5 mL of $SnCl_2{\cdot}2H_2O$ with

5 mL of triethanolamine was added. These compounds were also added in a 50 mL glass beaker and placed in a magnetic mixing device (magnetic stirrer). The color of the solution quickly changes to white as monitored. In addition, 2 mL of sodium hydroxide solution was then added to 3 mL of polyphenol alcohol. The addition is gradual and sequential at continued mixing. The reaction of sol and deionized water was mixed slowly at room temperature at continuous stirring. Thus, the substrates were vertically dipped into the sol in a beaker containing the mixed reaction. The beaker was placed in a water bath at a temperature of 80 ± 3°C. The solution was stirred with a magnetic stirrer. Then, it was annealed with continued stirring to the required heat of deposition. The pH was measured by pH meter type (Hana, pH211 Digital). The measured pH at the start of the deposition process was 9. Substrates were then removed after a suitable time. They were washed with distilled water, and then dried. Subsequently, they were subjected to heat treatment at 300°C, 400°C, and 500°C for 60 min.

2.3. *Characterization of nanocrystalline SnO_2 films*

The crystal structure of SnO_2 films was analyzed using X-ray diffraction (XRD) system (Shimadzu X-ray diffraction) with CuKα_1 radiation at $\lambda = 1.54$ Å, 30 kV, and 30 mA. Film thickness was measured by interferometry Fizeau using a He–Ne laser (0.632 μm). The morphologies of the resulting films were characterized by atomic force microscopy (AFM) (CSPM-5000) and scanning electron microscopy (SEM) (VEGA TE Scan). The optical transmittance and absorbance measurement were performed with UV/Vis spectrophotometer (UV-1800 Shimadzu) with double beam at a wavelength range from 300–1000 nm.

3. Results and Discussion

3.1. *XRD analyses*

The XRD spectra revealed the crystalline growth of SnO_2 films produced through dip coating and CBD techniques on clean glass substrates at various annealing temperatures of 300°C, 400°C, and 500°C for 60 min in air. The influence of annealing temperature on the crystallinity of SnO_2 prepared by dip coating is illustrated in Fig. 1(a). X-ray analysis displayed well-defined diffraction peaks with good crystallinity. The diffraction peaks are in good agreement with those given in JCPD data card (JCPDS No. 41–1445). Each annealed sample is polycrystalline with a tetragonal crystal composition. The polycrystalline and film prefer the growth direction along (110). Other peaks corresponding to the directions of (101), (200), (211), and (220) are also observed. An increase in annealing temperature improves the crystal structure by increasing the intensity of the planes. This improvement in crystal structure can be due to the increasing size of crystallite as small crystallites aggregate in the planes with the increasing annealing temperature (Table 1). Annealing thin films at a temperature of 500°C shows a strong preferential growth orientation along the (110) plane.

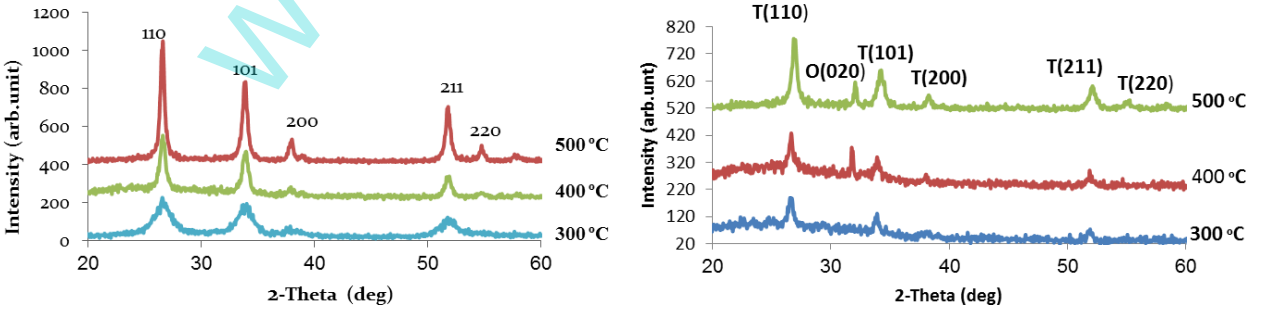

(a) (b)

Fig. 1. XRD patterns of SnO_2 thin films at various annealing temperatures and constant annealing time of 60 min (a) by dip coating and (b) by CBD.

Table 1. Obtained results of the XRD for SnO_2 thin films at various annealing temperatures and constant annealing time of 60 min.

	Annealing temperatures (°C)	(2θ)(deg)	hkl	FWHM β (deg)	d(Å) XRD	d(Å) JCPDS	a(Å)	c(Å)	Average grain size (nm)
Dip Coating									
	300	26.58	(110)	0.9980	3.3363	3.347	4.738	3.18	8
	400	26.62	(110)	0.5651	3.3215	3.347	4.78	3.174	14
	500	26.6	(110)	0.3650	3.3470	3.347	4.763	3.2	22.34
CBD									
	300	26.65	(110)	1.3542	3.361	3.347	4.738	3.19	10
	400	26.7	(110)	0.5441	3.359	3.347	4.73	3.22	15
	500	26.8	(110)	0.3720	3.3562	3.347	4.743	3.3	22

The diffraction peaks of the films become sharp, in turn, leading to increase in the crystalline films. The full width at half maxima (FWHM) decreases with the increase of annealing temperature. These results agree with the previous results.[12–19] The size of crystalline of film is calculated by Scherrer–Debye formula[20]:

$$D = 0.9\lambda/\beta\cos\theta, \tag{1}$$

where λ, β, and θ represent the wavelength of X-ray (1.541 Å), FWHM, and Bragg angle, respectively. The size of crystalline was 8, 14, and 22.34 nm at 300°C, 400°C, and 500°C, respectively. The influence of annealing temperature on the crystallinity of SnO_2 films produced by CBD technique can be understood from Fig. 1(b). When the annealing temperature is 300°C, four different located peaks corresponding to 110, 101, 200, and 211 planes were observed. The tensile stress could have resulted from the oxygen vacancies in the lattice of SnO_2 crystallites in the film as the annealing temperature rises up to 400°C, the peaks associated with the tetragonal phase, and the presence of the (020) reflections corresponds to orthorhombic phase due to the tensile stress in SnO_2.[20] At an annealing temperature of 500°C, five different located peaks corresponding to tetragonal 110, 101, 200, 211, and 220 planes and (020) reflection corresponding to orthorhombic phase are observed. Increase in intensity of (110) orientation becomes sharp and intense. This finding indicated that crystallinity was improved because annealing temperature provides energy for the atoms on the film to enhance mobility that can decrease defects in SnO_2 films and improve their quality. Thus, the FWHM of the peak is reduced and the size of the crystallites of the films is increased. These results agree with previous findings.[21] The crystalline sizes calculated using Eq. (1) were 10, 15, and 22 nm at 300°C, 400°C, and 500°C, respectively.

3.2. *AFM analyses*

Figure 2 reveals the 2D and 3D AFM images of SnO_2 thin films produced by using dip coating deposited at an annealing temperature of 300°C, 400°C, and 500°C at an annealing time of 60 min on a cleaned glass substrate. This surface property is important for applications, such as gas sensing. AFM images show that all films are well faceted crystallites, uniformly packed, and with small grain. Grain size increases as annealing temperature increases. The histogram of size distance shows the size of particle ranging from 70 nm to 91.67 nm. The roughness of surface decreases with increasing annealing temperature, wherein the relationship of grain size with the roughness is an inverse relationship as shown in Table 2. Figure 3 reveals the 2D and 3D AFM images of SnO_2 thin films prepared by CBD and deposited at an annealing temperature of 300°C, 400°C, and 500°C at an annealing time of 60 min on cleaned glass substrate. The small particles are arranged closely as can be observed from AFM image of the SnO_2 thin films annealed at 300°C. Meanwhile, the AFM image of the SnO_2 thin films annealed at 400°C shows larger particles formed in the film compared with the films annealed at 300°C. A topographical scan of SnO_2 films annealed at 500°C exhibits a regular pattern of pore walls and pore openings in the film, with well-defined boundaries of grain. These results indicate that annealing temperature exhibits a strong effect on the growth properties of film, such as size and shape of particles. The roughness of these films decreases

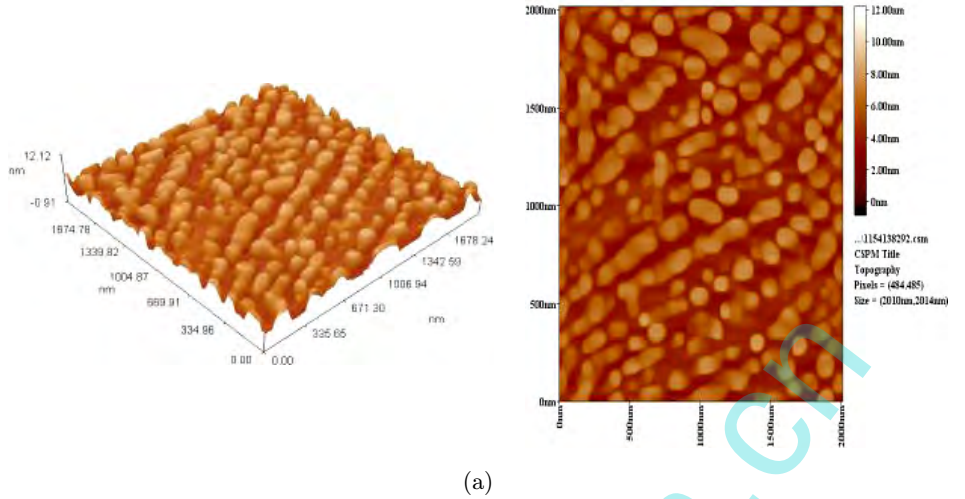

(a)

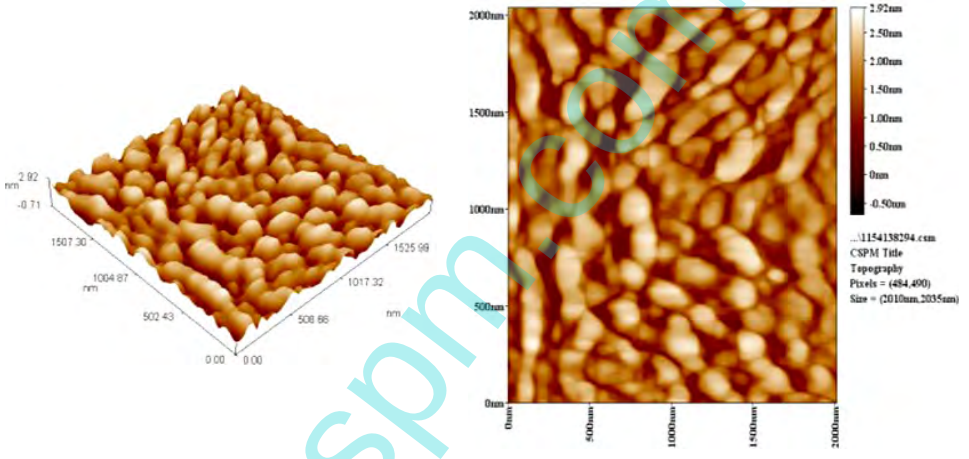

(b)

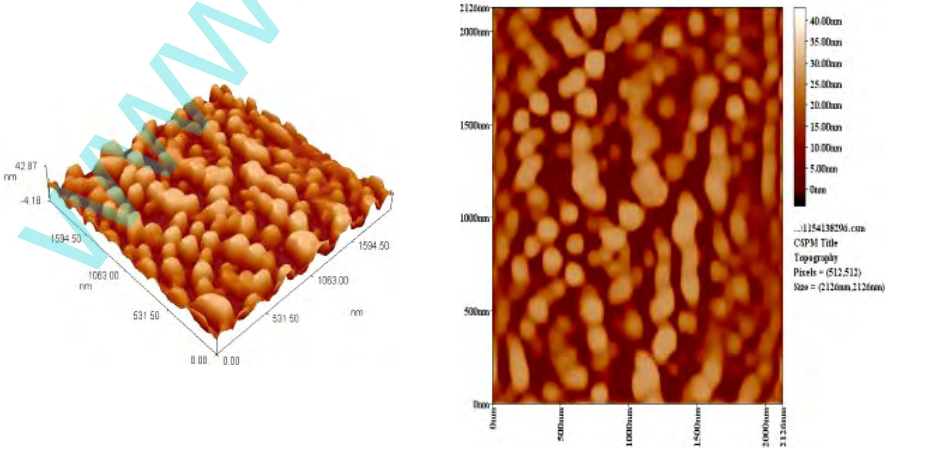

(c)

Fig. 2. Two- and three-dimensional AFM images of SnO_2 thin films prepared by using dip coating at various annealing temperatures of (a) 300°C, (b) 400°C, and (c) 500°C.

Table 2. Variation of root mean square, roughness, and grain size of SnO_2 from AFM, SEM, and XRD at various annealing temperatures.

	Annealing temperature(°C)	Grain size (nm) AFM	Grain size (nm) SEM	Grain size (nm) XRD	Roughness (nm)	RMS (nm)
Dip coating						
	300°C	70.	27.95	8	8.93	10.3
	400°C	80.38	44.12	14	2.77	3.21
	500°C	91.67	79.22	22.34	1.01	1.17
CBD						
	300°C	80.5	43.11	10	2.11	2.55
	400°C	85.2	50.76	15	1.2	1.38
	500°C	88.56	61.62	22	1.12	1.3

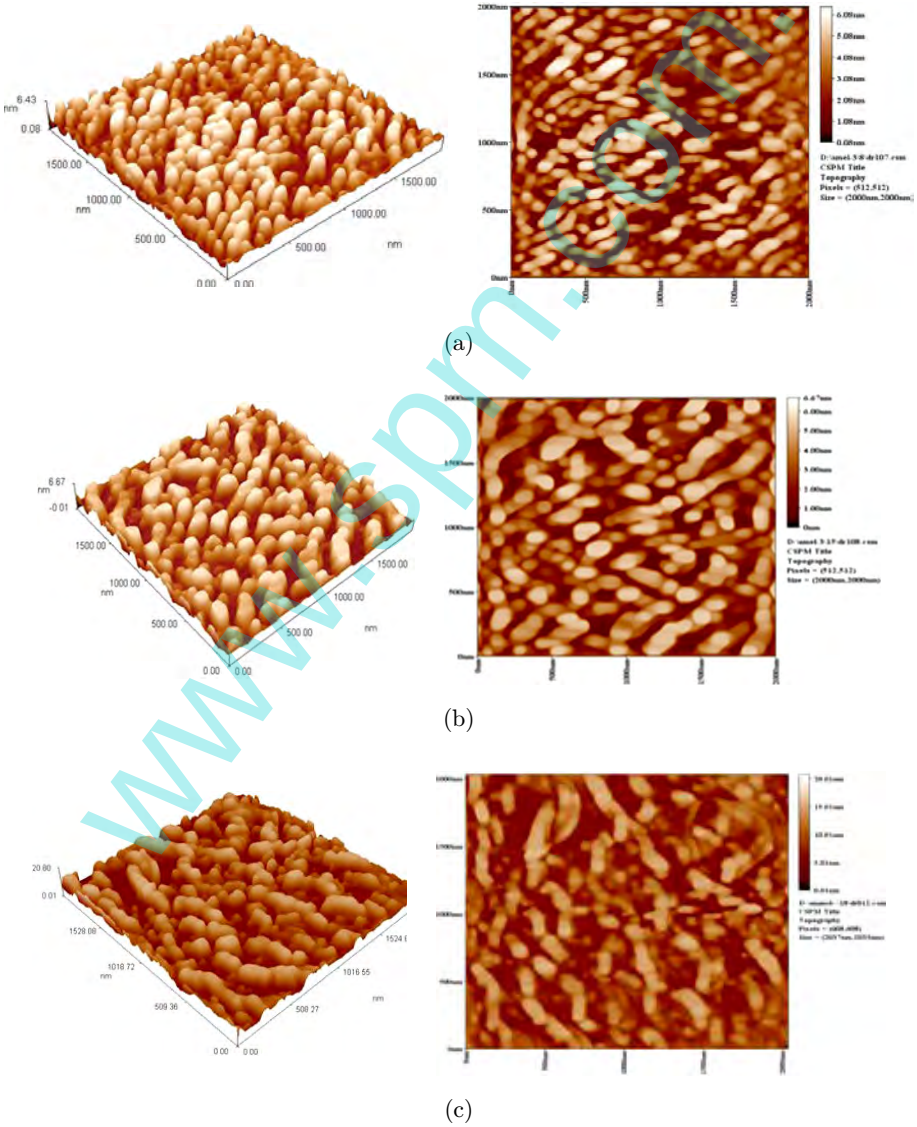

Fig. 3. Two- and three-dimensional AFM images of SnO_2 thin films prepared by using CBD at various annealing temperatures of (a) 300°C, (b) 400°C, and (c) 500°C.

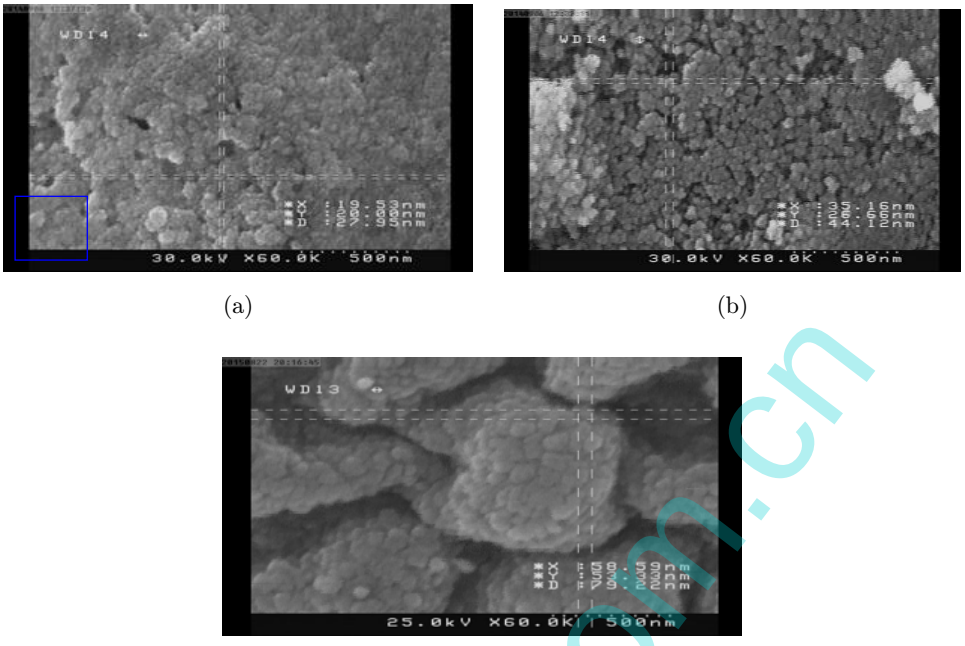

(a) (b)

(c)

Fig. 4. SEM image (top view) of SnO_2 film prepared by dip coating at annealing temperature of (a) 300°C, (b) 400°C, and (c) 500°C.

with the increase of annealing temperatures; these results agree with previous findings.[18]

3.3. *SEM analyses*

Figure 4 shows the SEM images that feature morphology of surface of the SnO_2 thin films produced by using dip coating on a clean glass substrate at various annealing temperatures. The SEM photograph illustrates the tightly packed grains. Furthermore, all of the films exhibit a homogeneous, uniform surface morphology that is dense and adhere well to the substrate without any cracks. The sizes of grains obtained from SEM images are 27.95, 44.12, and 79.22 nm at annealing temperatures of 300°C, 400°C, and 500°C, respectively. The increasing of size of particle with increase in annealing temperatures is caused by reduction of boundaries of grain in SnO_2 thin film as noted from the SEM. These results agree with XRD results. Figure 5 shows that the SEM images are the featured morphology of surface of the SnO_2 thin films produced by CBD on cleaned glass substrate at various annealing temperatures. The SEM photograph clearly illustrates the tightly packed grains. Furthermore, all the films are homogeneous surface morphology, dense with few porosities, and adhere well to the substrate without any cracks. The sizes of grains gained from SEM are 43.11, 50.76, and 61.62 nm at annealing temperatures of 300°C, 400°C, and 500°C, respectively. The increase in particle size is due to increasing annealing temperature as seen from the SEM. These results are consistent with the XRD results. The particle size shown by AFM and SEM is higher than that calculated from the XRD results because XRD provides the average mean crystallite size, whereas AFM and SEM show the probable grain aggregate of many crystallites.

3.4. *Optical properties*

3.4.1. *Transmission*

All of the films exhibited uniform thickness, although their optical properties remain unchanged as their position is altered. The influence of various annealing temperatures at 300°C, 400°C, and 500°C at constant annealing time of 60 min on SnO_2 thin films produced by using dip coating and CBD is shown in Fig. 6. The SnO_2 film exhibits high transmission in the entire visible region (i.e. above 400 nm). As annealing temperature increases, optical transmission

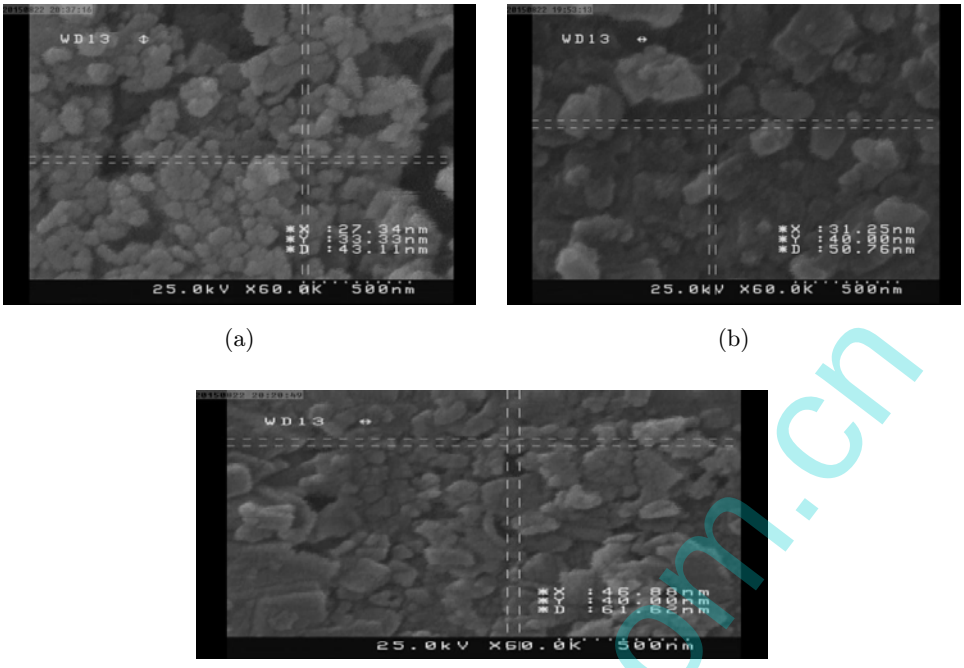

(a) (b)

(c)

Fig. 5. SEM image (top view) of SnO_2 film prepared by CBD at annealing temperatures (a) 300°C, (b) 400°C, and (c) 500°C.

also increases. This finding is attributed to the increase in film homogeneity and degree of film crystallinity. Our results are consistent with previous findings.[8,18,19]

3.4.2. *Optical energy gap*

The band gaps of these films were calculated from the equation.[22]

$$\alpha h\upsilon = A(h\upsilon - E_g)^r, \tag{2}$$

where α is the coefficient of absorption; h is the Planck's constant; υ is the frequency of fallen light; E_g is the optical energy gap of the material; r is the factor controlling the direct and indirect transitions of the electrons from the valence band to the conduction band, and where A is fixed. $h\nu$ is the energy of photon. The value of optical energy gap (E_g) is

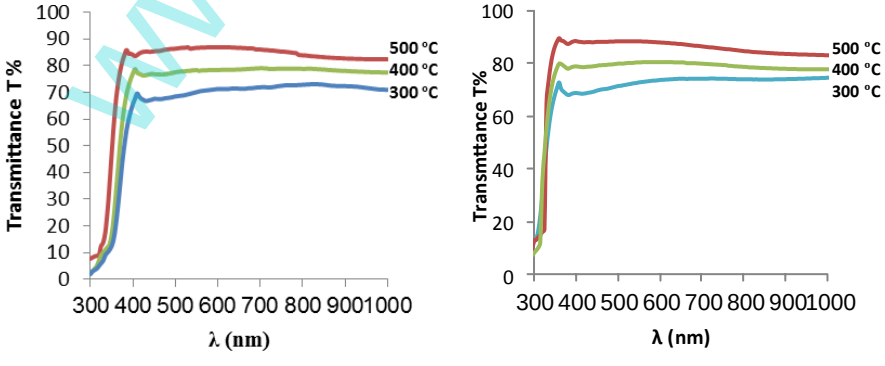

(a) (b)

Fig. 6. Variation of transmittance with wavelength of SnO_2 thin films at various annealing temperatures (a) by dip coating and (b) by CBD.

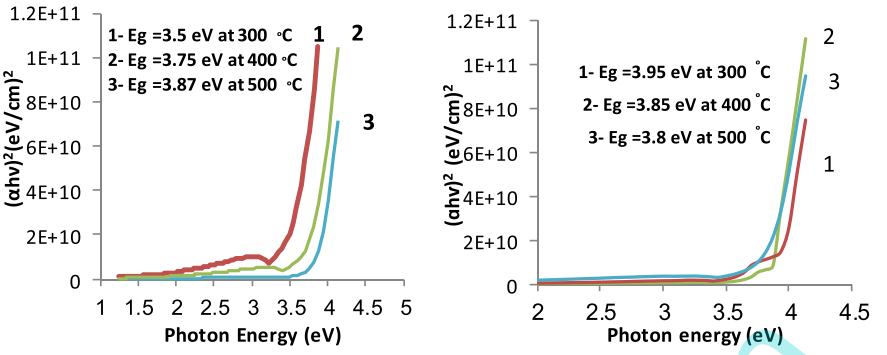

Fig. 7. Variation of $(\alpha h\upsilon)^2$ vs $(h\upsilon)$ for SnO_2 films for various overheat temperatures (a) by dip coating and (b) by CBD.

studied by extrapolation of the straight line of the plot of $(\alpha h\upsilon)^2$ with energy of photon for various annealing temperatures of SnO_2 thin films produced by using dip coating as shown in Fig. 7(a). The linear dependence of $(\alpha h\upsilon)^2$ with $(h\upsilon)$ indicates direct band gap. The results show that the annealing temperature is very important in the optical band gap assignment. The optical energy band gap is increased from 3.5 eV to 3.87 eV with the increasing annealing temperature from 300°C to 500°C as shown in Table 3. This result may be due to the removal of defects of surface with annealing. Another reason is that optical band gap increases with annealing. This phenomenon is possibly associated with the increase in grain size and the decrease in the density of defects and number of boundaries (improving crystallinity as shown by X-ray, Fig. 1(a)). These results are in agreement with previous results.[18,23,24] Meanwhile, SnO_2 thin films prepared by CBD are shown in Fig. 7(b). The optical band gap energy is reduced from 3.95 eV to 3.8 eV at increasing annealing temperature from 300°C to 500°C as shown in Table 3. The band gap is reduced due to the reduction in the transition tail width and shift effect. These results are in agreement with previous results.[25–27]

3.5. *Electrical conductivity*

The electrical conductivity of SnO_2 thin films was measured at a temperature range from 303–433 K. The electrical conductivity increases exponentially as the temperature increases as noticed in all SnO_2 films. This finding represents common semiconductor property (the charge carrier concentration increases when the temperature increases). Figure 8 shows the relationship between $\ln\sigma$ and $1000/T$ at different annealing temperatures of SnO_2 films prepared by dip coating and CBD technique. The figure shows two mechanisms of conductivity elevation to the two energies of activation E_{a1} and E_{a2}. The first energy of activation (E_{a1}) occurs at high temperatures. This phenomenon is the reason for conduction of the carrier excited into the expanded states after the mobility edge. Meanwhile, the second activation energy (E_{a2}) is observed at low temperatures. The conduction mechanism of this step is the reason of carrier transfer to the location near to states of the valence and band of conduction. With the annealing temperature increasing, the electrical conductivity increases (Fig. 8); this finding may be due to the increase in the concentration of charge carriers' due to the increase in vacancies of oxygen by increasing the

Table 3. Values of optical energy gap of SnO_2 thin films prepared by using dip coating and CBD techniques.

Method	Annealing temperature	E_g(eV)	Method	Annealing temperature	E_g(eV)
Dip coating	300°C	3.5	CBD	300°C	3.95
	400°C	3.75		400°C	3.85
	500°C	3.87		500°C	3.8

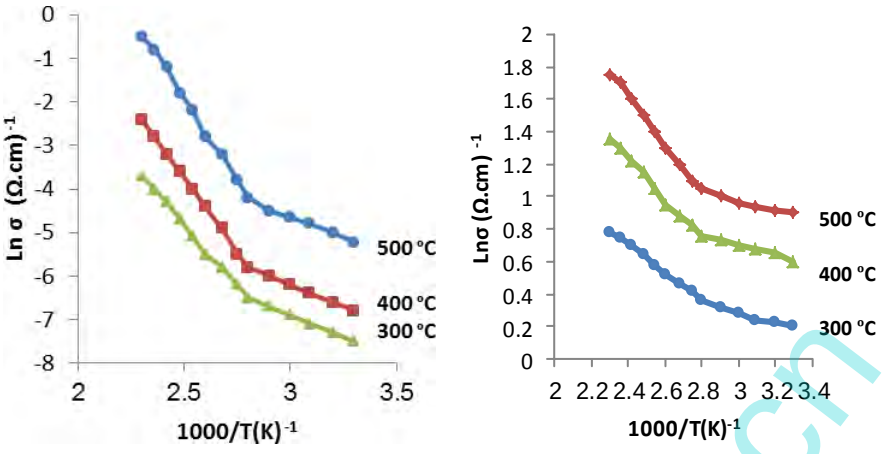

(a) (b)

Fig. 8. Ln σ as a function of $1000/T(\mathrm{K})^{-1}$ for SnO_2 films at various annealing temperatures (a) by dip coating and (b) by CBD.

annealing temperature.[28] In addition, the boundaries of the grains spread with rise in the annealing temperature. This phenomenon results in an increase in grain size and electrical conductivity. The energy activation is calculated using the formula[29]:

$$\sigma = \sigma_{\circ}\exp(E_a/kT), \tag{3}$$

where σ is the conductivity at heat T; σ_o is fixed; k is the constant of Boltzmann; T is the absolute of temperature and E_a is the activation energy. The activation energy indicates the site n of trap levels below the band of conduction. From Fig. 8, energy of activation (E_a) increases when film is annealed at 300°C, 400°C to 500°C for both films prepared by dip coating and CBD. Table 4 shows the activation energies E_{a1} and E_{a2} of the SnO_2 thin films prepared by dip coating and CBD.

Table 4. Activation energies E_{a1} and E_{a2} for SnO_2 thin films at various annealing temperatures prepared by using dip coating and CBD.

Annealing temperatures		Activation energy E_{a1}(eV)	Activation energy E_{a2}(eV)
Dip coating	300°C	0.4	0.025
	400°C	0.45	0.03
	500°C	0.5	0.035
CBD	300°C	0.09	0.02
	400°C	0.11	0.03
	500°C	0.15	0.043

3.6. *Sensing properties*

Gas sensing reactions are due to surface sensitivity. An increase in surface area attributed to nanosized films increases the probability of these reactions and hence sensitivity. When the surface of SnO_2 thin films is exposed to air, an electron depletion layer is formed because of absorbance. In this layer, electron density is low, and a high-resistance layer is consequently established. In addition, the adsorbed oxygen remains in the form of O^- and O_2^- species. Thus, high-resistance SnO_2 thin film is present in air. More electrons are released when the surface of SnO_2 thin film is exposed to the reducing gas CO because of surface reaction. These released electrons transfer back into the conduction band, which increases the conductivity or decreases the resistance of SnO_2 films.[9,30] The sensitivity of SnO_2 thin films to CO gas was studied at a concentration of 50 ppm. The sensitivity S of SnO_2 gas sensor is typically explained as the rate of the surface resistance R_a of the film in air to that in the target gas (R_g)[22]:

$$S = \left|\frac{R_g - R_a}{R_a}\right| \times 100. \tag{4}$$

The sensitivity of SnO_2 thin films produced by using dip coating and CBD on a clean glass substrate at various annealing temperatures with operating time at room temperature is shown in Figs. 9(a) and 9(b). The sensitivity of all of the samples to CO decreases as annealing temperature increases.

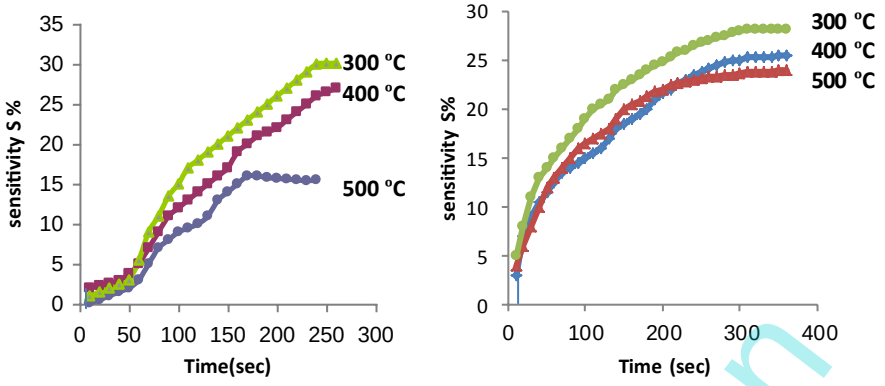

(a) (b)

Fig. 9. Sensitivity (S) as a function of time plot of SnO_2 thin films at various annealing temperatures deposited (a) by dip coating and (b) by CBD.

The decreasing in the sensitivity in this case may be the reason for the influence of the change in the size of particle,[27,31] where the sensor samples with small particles exhibit high surface region providing further efficient sites at which the gaseous species adsorb and interact as the average size of particle of the sensor samples increases with annealing temperature. The sensitivity of the samples prepared by dip coating annealed at 300°C and 400°C is higher to gas sensing than that of the samples prepared by CBD because of an increase in surface area attributed to their small grain size. Meanwhile, the films prepared by CBD and annealed at 500°C showed higher sensitivity than the films produced by using dip coating at the same annealing temperature because of small grain size as shown in XRD results. Response time and recovery time are the basic parameters of the gas sensors. The response time is defined as the time taken by the sensor to attain 90% of maximum change in resistance on exposure to gas; the recovery time is defined as the time taken by the sensor to obtain 90% of the original resistance.[32] In Fig. 9, the SnO_2 films produced by using dip coating annealed at 500°C show a response time of 175 s. Meanwhile, SnO_2 films produced by using CBD and annealed at 500°C exhibit a response time of 280 s. Similarly, the recovery time (τ_{rec}) is defined as the time required to recover within 10% of the original baseline when the flow of reducing or oxidizing gas is removed.

Figure 10 shows the sensitivity to CO gas as a function of temperature of SnO_2 thin films produced by using dip coating and CBD at various annealing

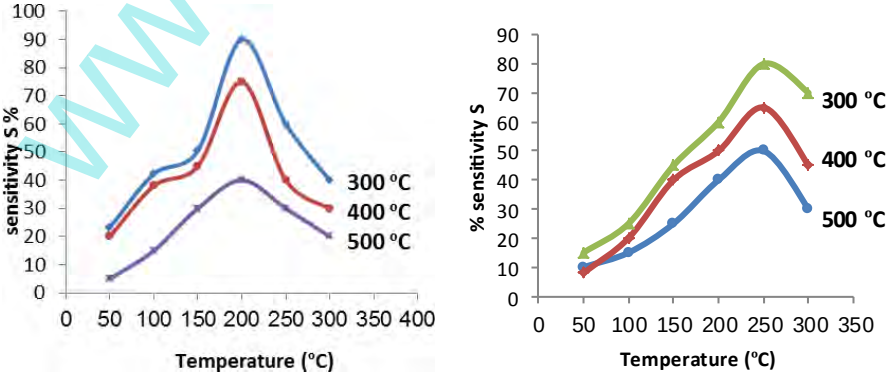

(a) (b)

Fig. 10. Sensitivity (S) as a function of temperature plot of SnO_2 thin films at different annealing temperatures for CO gas (a) by dip coating and (b) by CBD.

temperatures of 300°C, 400°C, and 500°C. The sensitivity gradually increases with increasing temperature and attains the ultimate values at 200°C for samples prepared by dip coating, and 250°C for samples prepared by CBD. With the temperature increasing above 200°C or 250°C, the sensitivity of the sensor samples decreased. The high sensitivity of the sensor samples to CO gas at 200°C or 250°C can be explained depending on gas adsorption models, in which the sensitivity of sensor samples depends on the interaction between the adsorbed oxygen species and CO on their surfaces.[33] As the temperature of the sensor samples increases above 50°C, the concentration of the adsorbed oxygen species gradually increases at a certain temperature by accepting electrons from the conduction band. This phenomenon is accompanied by an increase in electrical resistance. Thus, maximum sensitivities were obtained at 200°C or 250°C because of the high density of the chemisorbed oxygen kinds and the high oxidation action of CO. At temperatures higher than 200°C or 250°C, oxygen species from the sensor surfaces are adsorbed and their densities are decreased. Consequently, sensitivity decreases.

4. Conclusions

Low-cost, simple, and efficient methods have been used to fabricate CO gas sensors composed of SnO_2. In our study, the structural, optical, and electrical properties of SnO_2 thin films were examined. XRD, AFM, and SEM revealed that the grain size of CBD-synthesized films is larger than that of dip-coated films at annealing temperatures of 300°C and 400°C. By comparison, the grain size of the former is smaller than that of the latter at 500°C. The films were then exposed to CO to determine their gas sensing properties. Our results showed that the dip-coated and CBD-prepared films are highly sensitive to 50 ppm CO at 200°C and 250°C, respectively. Therefore, the gas sensing properties of dip-coated SnO_2 films are higher than those of CBD-prepared films because the former possesses larger surface areas available for exposure than the latter does.

References

1. N. A. A. Al-Tememee, M. A. Hmeed and F. T. Ibrahim, *Int. J. Curr. Eng. Technol.* **4** (2014) 516.
2. A. Ayeshamariam, *J. Photon. Spintron.* **2** (2013) 4.
3. R. T. Jacob, J. Thomas, R. George, M. Kumaran, and G. Vardhan, *Int. J. Res. Eng. Technol.* **38** (2014) 599.
4. M. K. M. Ali, K. Ibrahim, O. S. Hamad, M. H. Eisa, M. G. Faraj, and F. Azhari, *Rom. J. Phys.* **56** (2011) 730.
5. C. M. Wang, C. C. Huang, J. C. Kuo, D. R. Sahu and J. L. Huang, *Materials* **8** (2015) 5289.
6. P. P. Hao, C. L. Chen, Y. L. Wet and X. H. Mu, *Chin. J. Inorg. Chem.* **30** (2014) 451.
7. I. H. Kadhim and H. A. Hassan, *J. Appl. Sci. Agric.* **10** (2015) 159.
8. B. W. Shivaraj, H. N. N. Murthy, M. Krishna and B. S. Satyanarayana, *Procedia Mater. Sci.* **10** (2015) 292.
9. Y. Liu, E. Koep and M. Liu, *Chem. Mater.* **17** (2005) 3997.
10. P. M. Mwathe, R. Musembi, M. Munji, F. Nyongesa, B. Odari, W. Njoroge, B. Aduda and B. Muthoka, *Adv. Mater.* **4** (2015) 51.
11. H. U. Igwe and E. I. Ugwu, *Adv. Appl. Sci. Res.* **1** (2010) 240.
12. M. Caglar and K. C. Atar, *Mol. Biomol. Spectrosc.* **96** (2012) 882.
13. G. F. Fine, L. M. Cavanagh, A. Afonja and R. Binions, *Sensors* **10** (2010) 5469.
14. R. S. Khadayate and P. P. Patil, *J. Optoelectron. Adv. Mater.* **12** (2010) 1338.
15. E. W. Williams, N. Tomlinson, M. T. Cheney and A. G. Keeling, *J. Mater. Sci. Mater. Electron* **11** (2000) 369.
16. S. K. Tripathy, and B. P. Hota, *Afr. Rev. Phys.* **7** (2012) 401.
17. M. R. Vaezi and M. Zameni, *J. Ceram. Process. Res.* **13** (2012) 778.
18. A. Khan, M. Mehmooda, M. Aslam and M. Ashraf, *Appl. Surf. Sci.* **256** (2010) 2252.
19. J. Joseph, M. Varghese and M. Jacob, *Turk. J. Phys.* **33** (2009) 37.
20. J. Liu, D. Wu and S. Zeng, *J. Mater. Process. Technol.* **209** (2009) 3943.
21. M. A. Camacho-Lopez, J. R. Galeana-Camacho, A. Esparza-Garcia and C. Sanchez-Pérez, *Superficies Vacío* **26** (2013) 95.
22. C. H. Liu, L. Zhang and J. H. Yuan, *Thin Solid Film*, **304** (1997) 13.
23. V. Arivazhagan and S. Rajesh, *J. Ovonic Res.* **6** (2010) 221.
24. S. Abdullahi, A. U. Moreh, B. Hamza, M. A. Wara, H. Kamaluddeen, M. A. Kebbe and U. F. Monsuorat, *Int. J. Recent Res. Phy. Chem. Sci.* **1** (2015) 1.
25. M. G. Varnamkhasti, H. R. Fallah and M. Zadsa, *Vacuum* **86** (2012) 871.
26. W. Azydorczyk, K. Waczýnski and J. Zydorczyk, *Mater. Sci.-Poland* **3** (2014) 729.
27. R. A. Ismail, S. M. H. Al-Jawad and N. Hussein, *Appl. Phys. A* **117** (2014) 1977.

28. M. E. M. Hassouna, A. M. El-Sayed, F. M. Ismail, M. H. Khder, A. A. Farghali and S. M. Yakout, *Int. J. Nanomater. Bios.* **2** (2012) 44.
29. R. D. Sakhare, G. D. Khuspe, S. T. Navale, R. N. Mulik, M. A. Chougule, R. C. Pawar, C. S. Lee, S. Sen and V. B. Pati, *J. Alloys Compd.* **563** (2013) 300.
30. P. Sagar, M. Kumar and R. M. Mehra, *Mater. Sci-Poland* **23** (2005) 685.
31. R. C. Singh, M. P. Singh, O. Singh and P. S. Chandi, *Sens. Actuators* **143** (2009) 226.
32. G. H. Jain, L. A. Patil, M. S. Wagh, D. R. Patil, S. A. Patil, and D. P. Amalnerkar, *Sens. Actuators B* **117** (2006) 159.
33. A. R. R. Kumar, O. Al-Dossary, G. Kumar and A. Umar, *Nano-Micro Lett.* **7** (2015) 97.